Optik - International Journal for Light and Electron Optics 218 (2020) 164879

Contents lists available at ScienceDirect

Optik

journal homepage: www.elsevier.com/locate/ijleo

Original research article

All-optical OR and NOR gates using quantum-dot semiconductor optical amplifiers-assisted turbo-switched Mach-Zehnder interferometer and serially delayed interferometer at 1 Tb/s

Amer Kotb[a,b,*], Chunlei Guo[a,c,*]

[a] The Guo China-US Photonics Laboratory, Changchun Institute of Optics, Fine Mechanics, and Physics, Chinese Academy of Sciences, Changchun 130033, China
[b] Department of Physics, Faculty of Science, University of Fayoum, Fayoum 63514, Egypt
[c] The Institute of Optics, University of Rochester, Rochester, NY 14627, USA

ARTICLE INFO

Keywords:
All-optical OR gate
All-optical NOR gate
Quantum-dot semiconductor optical amplifier
Turbo-switch
Mach-Zehnder interferometer
Delayed interferometer

ABSTRACT

The turbo-switch (TS) has proven to enhance the speed of the conventional semiconductor optical amplifier (SOA) up to four times better than the single SOA architecture. A novel performance of all-optical (AO) OR and NOT-OR (NOR) logic gates using TS Mach-Zehnder interferometer (TSMZI) combined with the ultrafast quantum-dot (QD) SOAs and followed by a serially delayed interferometer (DI) is numerically analyzed and investigated at 1 Tb/s. For comparison, the results have been obtained for AO OR and NOR Boolean functions using a DI after QDSOAs-based TSMZI, QDSOAs-based TSMZI, and QDSOAs-based conventional MZI. The achieved results indicate that placing a DI in series with the QDSOAs-TSMZI renders acceptable of OA OR and NOR operations at 1 Tb/s than QDSOAs-TSMZI and QDSOAs-MZI, where this achievement is not possible.

1. Introduction

Semiconductor optical amplifiers (SOAs) have been attracted a huge number of interests in recent years as one of the key nonlinear elements for optical signal processing due to their strong nonlinearity, low power consumption, wide bandwidth, compact size, and ease of scalable integration in single chips with the other optoelectronic devices at affordable prices. Despite these attractive advantages, the exploitation of SOAs in applications of ultrafast all-optical (AO) logic gates is limited by the finite SOA carrier recovery time (i.e., ~ 100 ps), which results in a pattern-effect and then performance degradation at higher bit rates [1]. In order to directly overcome the speed limitation of the SOA carrier relaxation time, two notable paths have been used to face this problem include (1) placing quantum-dots (QDs) in the SOAs active region in order to directly overcome the speed limitation of the SOA carrier relaxation time. In recent years, QDSOAs have widely been employed for the applications of the AO signal processing with the pattern-free performance [2–18] owing to their low threshold current, high saturation power, wide bandwidth, temperature insensitivity, low chirp [19–22] and, above all, faster gain recovery time [23] (i.e., 300 fs-10 ps) than bulk and quantum-well SOAs. (2) Turbo-switch (TS) incorporated a pair of cascaded SOAs and separated by a wide optical filter (OF) [24–31], which is used to filter out the pump pulses and pass only the modulated continuous wave (CW) probe beams to the second SOA, is another solution to confront the SOA limitation problem. The TS has proven to enhance the speed of the conventional SOA up to four times better than

* Corresponding authors.
E-mail addresses: amer@ciomp.ac.cn (A. Kotb), guo@optics.rochester.edu (C. Guo).

https://doi.org/10.1016/j.ijleo.2020.164879
Received 21 November 2019; Accepted 1 May 2020
Available online 21 May 2020
0030-4026/

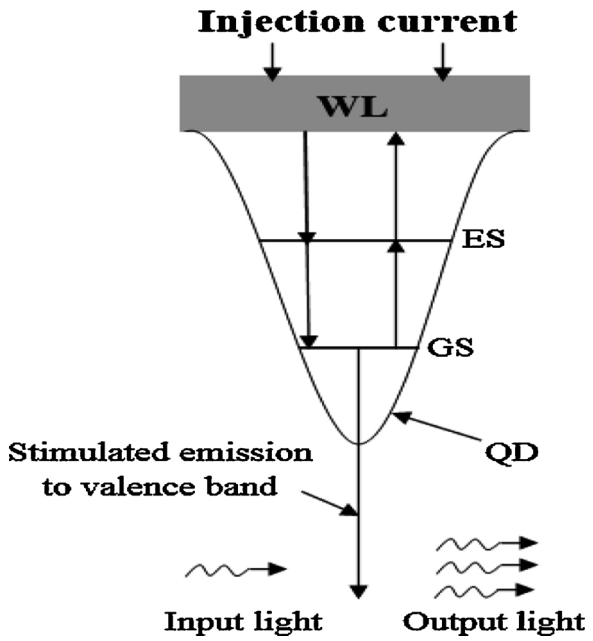

Fig. 1. Schematic diagram of QDs states and carrier transitions.

the single SOA architecture [28,29]. The TS is placed on both arms of Mach-Zehnder interferometer (MZI) where is easy to combine the structural simplicity and control the phase of the signal in each arm. Nevertheless, better results have been achieved when using this novel architecture, which is known as the turbo-switched Mach-Zehnder interferometer (TSMZI). In order to overcome the performance degradation of the AO gates, a delay interferometer is serially connected with TSMZI resulting in a better performance than if the TSMZI were not assisted by the delayed interferometer (DI) beneficial action [32–34]. The DI creates a phase window whose duration is determined by the DI shorter delay [35], thus overcoming the negative impact on output signal quality. In this article, we continue and extend our previous relevant work on 1 Tb/s AO XOR and AND operations using QDSOAs-based TSMZI [36] by studying a novel realization of the fundamental AO OR and NOT-OR (NOR) logic gates using QDSOAs-based TSMZI followed by a series DI at 1 Tb/s. Moreover, the variation of gates' quality factor (QF) against the input signal and QDSOA critical parameters has been examined and assessed. For comparison, the results have been obtained for the AO OR and NOR gates using QDSOAs-based TSMZI followed by a serially DI, QDSOAs-based TSMZI, and QDSOAs-based MZI at 1 Tb/s. The obtained results demonstrate indeed the feasibility of using a serially DI after the QDSOA-based TSMZI scheme to execute the target Boolean functions at 1 Tb/s with better performance than the other schemes. Our task is to point out to a faster-response new nonlinear element to be used in more advanced and efficient photonic circuits.

2. Theoretical formulation

2.1. QDSOA rate equations

The semiconductor materials used to construct the QDSOA device are commonly InAs/GaAs where InAs QDs are embedded in a GaAs layer [2–5]. This device has a gain of ~ 15 dB and a low noise figure of ~ 7 dB at 1550 nm [4,5]. The schematic diagram of the QD states and carriers transitions using a two-level model in the QD conduction band is illustrated in Fig. 1. The electrical pump current is injected only via the wetting layer (WL) making the transition to the QD excited state (ES), which acts as a carrier reservoir for the QD ground state (GS), which has an ultrafast carrier relaxation time. The device gain is affected by the carrier densities and transition rates.

The following QDSOA rate equations describe the change in the carrier densities among a two-energy level, including the nonlinear intraband effects of carrier heating (CH) and spectral hole burning (SHB) [2,3,6–12,36]:

$$\frac{dh_d(t)}{dt} = \frac{h_w(t)}{\tau_{dw}}\left(1 - \frac{h_d(t)}{h_0}\right) - \frac{h_d(t)}{\tau_{dr}} - (\exp[h_d(t) + h_{CH}(t) + h_{SHB}(t)] - 1) \quad \frac{P_{in}(t)}{E_{sat}} \tag{1}$$

$$\frac{dh_w(t)}{dt} = \frac{h_{in}}{\tau_{wr}}(1 - \frac{h_w(t)}{h_0}) - \frac{h_w(t)}{\tau_{wr}} - \frac{h_w(t)}{\tau_{wd}}(1 - \frac{h_d(t)}{h_0}) \tag{2}$$

$$\frac{dh_{CH}(t)}{dt} = -\frac{h_{CH}(t)}{\tau_{CH}} - \frac{\varepsilon_{CH}}{\tau_{CH}}[\exp[h_d(t) + h_{CH}(t) + h_{SHB}(t)] - 1] \quad P_{in}(t) \tag{3}$$

$$\frac{dh_{SHB}(t)}{dt} = -\frac{h_{SHB}(t)}{\tau_{SHB}} - \frac{\varepsilon_{SHB}}{\tau_{SHB}}\left(exp\left[h_d(t) + h_{SHB}(t) + h_{CH}(t)\right] - 1\right)P_{in}(t) - \frac{dh_d(t)}{dt} - \frac{dh_{CH}(t)}{dt} \tag{4}$$

$$h_{in} = \int_0^z \frac{a\,J\tau_{wr}}{ed}\,dz' \tag{5}$$

where functions 'h' represent the QDSOA power gain integrated over its length for the carrier recombination between QDs states (h_d) and WL (h_w), carrier heating (h_{CH}), and spectral hole burning (h_{SHB}). $h_0 = \ln[G_0]$, where G_0 is the unsaturated power gain, E_{sat} is the saturation input energy, and $P_{in}(t)$ is the input pulse power injected into each QDSOA. τ_{dw} is the excitation rate from QD GS to WL and τ_{wd} is the transition rate from WL to QD GS. τ_{dr} and τ_{wr} are the carrier recombination rates of QD and WL, respectively. τ_{CH} and τ_{SHB} are the temperature relaxation rate and carrier-carrier scattering rate, respectively. ε_{CH} and ε_{SHB} are the nonlinear gain suppression factors due to CH and SHB, respectively. α is the differential gain, J is the injection current density, d is the WL thickness, and e is the electron charge.

The total gain of each QDSOA is given by [6–12]:

$$G_{QDSOA_i}(t) = \exp\left[h_d(t) + h_{CH}(t) + h_{SHB}(t)\right],\ \ i = 1, 2, 3, 4 \tag{6}$$

while the phase change of the probe wave propagated in each QSOA is given by [6–12]:

$$\Phi_{QDSOA_i}(t) = -0.5(\alpha\, h_d(t) + \alpha_{CH}\, h_{CH}(t)),\ \ i = 1, 2, 3, 4 \tag{7}$$

where α is the traditional linewidth enhancement factor (α-factor) and α_{CH} and α_{SHB} are the linewidth enhancement factors due to CH and SHB, respectively. The value of α_{SHB} is null in Eq. (7) because SHB achieves a nearly symmetrical spectral hole centered at the signal wavelength [7].

The time-domain input A, B, and clock (Clk) signals are assumed to be a Gaussian-shaped whose power profile is described as [2,3,36–38]:

$$P_{A,B,Clk}(t) \equiv P_{in}(t) = \sum_{n=1}^{N} a_{n(A,B,Clk)} \frac{2\sqrt{\ln[2]}\,E_0}{\sqrt{\pi}\,\tau_{FWHM}}\ exp\left[-\frac{4\ln[2](t - n\,T)^2}{\tau_{FWHM}^2}\right] \tag{8}$$

where $a_{n(A,B,Clk)}$ is the n-th bit slots of binary content '1' or '0' for signals A and B and '1' for the Clk signal inside $N = 2^7$-1 [31,36] bit-long pseudorandom binary sequence (PRBS) of pulses having energy, E_0, full-width at half-maximum pulse width, τ_{FWHM}, and bit period, T. The data pulse modulation format used in this simulation is a return-to-zero, which is widely employed in optical time-division multiplexing systems due to its attractive features of efficient tolerance to fiber nonlinearities and higher receiver sensitivity [39].

2.2. QDSOAs-based TSMZI followed by DI

The schematic diagram of QDSOAs-based TSMZI followed by a DI is shown in Fig. 2.

In this configuration, each arm of QDSOAs-TSMZI has two identical QDSOAs separated by an OF. The output components of QDSOA1 and QDSOA2 pass through OF1 and OF2, respectively, before entering the QDSOA3 and QDSOA4, which act as nonlinear optical filters to compensate for the finite recovery of the cross-modulated signal coming out of QDSOA1 and QDSOA2, respectively, thereby accelerating the overall nonlinear dynamical processes and resulting in considerably less pattern-dependent affected switching performance. The OF should be a Gaussian-shaped with a frequency-domain transfer function described by [31,36,40]:

$$OF_{1,2}(f) = \exp\left[-\ln\left[\sqrt{2}\right]\left(\frac{f - f_c}{B/2}\right)^{2N}\right] \tag{9}$$

where f is the input signal frequency, f_c is the OF center frequency, and B is the OF bandwidth. N is the OF order, which controls the

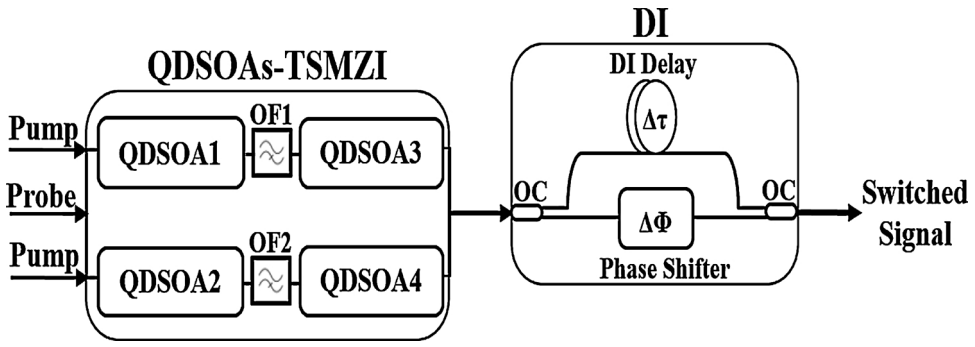

Fig. 2. Schematic diagram of QDSOAs-TSMZI with DI. OF: optical filter. OC: 3 dB optical coupler.

sharpness degree of the OF edges, where $N = 1$ corresponds to Gaussian and $N \geq 2$ to super-Gaussian shapes where the OF edges are steeper and the top of the OF is flatter [41].

The signal power inserted into QDSOA3 and QDSOA4 that is coming out of OF1 and OF2, respectively, is given by the square modulus of the complex electric field, $|E_{OF_{1,2}}(t)|^2$ [36,41]:

$$P_{in,QDSOA_{3,4}}(t) \equiv P_{OF_{1,2}}(t) = |E_{OF_{1,2}}(t)|^2 = |F^{-1}[F[E_{out,QDSOA_{1,2}}(t)] \cdot OF_{1,2}(f)]|^2 \tag{10}$$

where F and F^{-1} are the Fourier transform and its inverse, respectively. $E_{out,QDSOA_{1,2}}(t)$ is the complex electric field of the halved probe signal in QDSOA1 and QDSOA2, respectively [36,42]:

$$E_{out,QDSOA_{1,2}}(t) = \sqrt{0.5P_{probe}}\ \exp[0.5\ \ln[G_{QDSOA_{1,2}}(t)] + j\Phi_{QDSOA_{1,2}}(t)] \tag{11}$$

where P_{probe} is the probe input power and j is the imaginary unit.

The time-dependent output power of QDSOAs-TSMZI scheme is calculated by combining the complex electric fields and phases coming out of QDSOA3 and QDSOA4 at the TSMZI output port, i.e., [36,43]:

$$P_{out,TSMZI}(t) = 0.5(|E_{out,QDSOA_3}(t)|^2 + |E_{out,QDSOA_4}(t)|^2 + 2E_{out,QDSOA_3}(t)E_{out,QDSOA_4}(t)sin[\Phi_{out,QDSOA_3}(t) - \Phi_{out,QDSOA_4}(t)]) \tag{12}$$

with

$$E_{out,QDSOA_{3,4}}(t) = E_{OF_{1,2}}(t)\ \exp[0.5\ln[G_{QDSOA_{3,4}}(t)]\ ] \tag{13}$$

The DI is constructed by connecting two 3 dB optical couplers (OCs) with a length difference between the upper and lower arms that is equivalent to a relative time delay ($\Delta\tau$) [44]. The time-independent output power coming out of the DI is formulated as [34,44]:

$$P_{out,DI}(t) = 0.25(P_{out,TSMZI}(t) + P_{out,TSMZI}(t-\Delta\tau) - 2\sqrt{P_{out,TSMZI}(t)\,P_{out,TSMZI}(t-\Delta\tau)}\ cos[\Phi_{OR/NOR}(t) - \Phi_{OR/NOR}(t-\Delta\tau) + \Delta\Phi) \tag{14}$$

where $\Delta\tau$ is the DI delay and $\Delta\Phi$ is the DI phase bias. $\Phi_{OR/NOR}$ (t) is the QDSOAs-TSMZI phase response explicitly expressed by [34,44]:

$$\Phi_{OR/NOR}(t) = \Phi_{QDSOA_4}(t) - \arctan\left[\frac{\sqrt{G_{QDSOA_3}(t)/G_{QDSOA_4}(t)}\ \sin[\Phi_{QDSOA_3}(t) - \Phi_{QDSOA_4}(t)]}{1 - \sqrt{G_{QDSOA_3}(t)/G_{QDSOA_4}(t)}\ \cos[\Phi_{QDSOA_3}(t) - \Phi_{QDSOA_4}(t)]}\right] \tag{15}$$

On the other hand, when using a conventional QDSOA-MZI scheme, i.e. using only QDSOA1 and QDSOA2, the output power of MZI is described by [37,38]:

$$P_{out,MZI}(t) = 0.25\,P_{out}(t)\begin{pmatrix} G_{QDSOA_1}(t) + G_{QDSOA_2}(t) - 2\sqrt{G_{QDSOA_1}(t)\,G_{QDSOA_2}(t)} \\ cos[\Phi_{QDSOA_1}(t) - \Phi_{QDSOA_2}(t)] \end{pmatrix} \tag{16}$$

$G_{QDSOA1,2}$ and $\Phi_{QDSOA1,2}$ are known through Eqs. (6) and (7), respectively.

3. OR gate

3.1. Operation principle

The schematic diagram and truth table of AO OR gate using QDSOAs-based TSMZI in series with a DI is shown in Fig. 3. The time-dependent signal power inserted into QDSOAs 1 and 2 is, respectively, given by [47]:

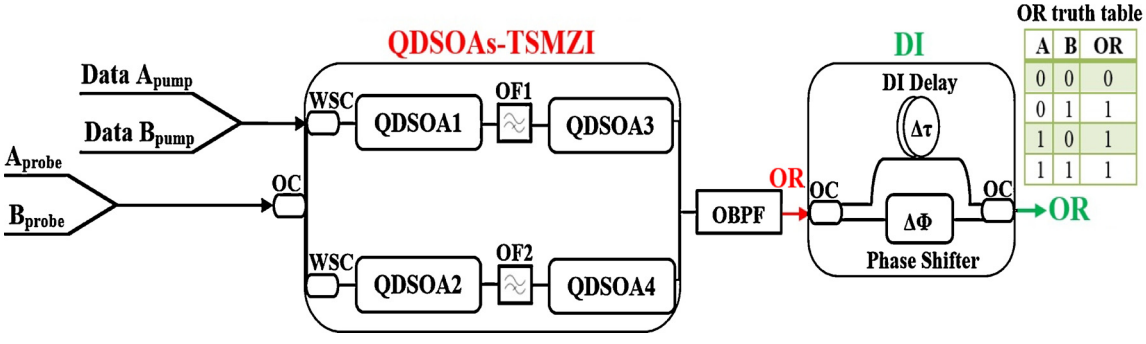

Fig. 3. Schematic diagram and truth table of OR gate using QDSOAs-based TSMZI in series with DI. OC: 3 dB optical coupler. WSC: wavelength-selective coupler. OF: optical filter. OBPF: 3 nm optical bandpass filter.

$$P_{in,\ QDSOA_1}(t) = P_{A_{pump}}(t) + P_{B_{pump}}(t) + 0.5\,(P_{A_{probe}}(t) + P_{B_{probe}}(t)) \quad (17)$$

$$P_{in,\ QDSOA_2}(t) = 0.5\,(P_{A_{probe}}(t) + P_{B_{probe}}(t)) \quad (18)$$

In order to investigate the OR operation, pump signals A and B as denoted by 'Data A_{pump}' and 'Data B_{pump}', respectively, are injected together via a wavelength-selective coupler (WSC) into the upper arm of the QDSOAs-TSMZI. While much lower signals of the same binary as denoted by 'A_{probe}' and 'B_{probe}' are divided in half by a 3 dB optical coupler (OC) and enter the middle arm of the QDSOAs-TSMZI. The nonlinear effects induced inside the QDSOAs by the pump signals are mapped and transformed into switching. The WSCs are chosen to exhibit low insertion losses and wide bandwidth in the optical communications C-band spectral region. The circuit operation relies on a cross-gain modulation (XGM) inside each QDSOA via the stronger pump signals, A_{pump} and B_{pump}, affecting the weaker probe counterparts, A_{probe} and B_{probe}, and relies subsequently on cross-phase modulation (XPM) incurred by the changes of the gain dynamics of the QDSOAs. Furthermore, when the combination $(A + B)_{pump}$ and $(A + B)_{probe}$ of the QDSOAs-TSMZI upper and lower arm, respectively, is '0', which happens when $A_{pump,\ probe}$ and $B_{pump,\ probe}$ are '0', the QDSOAs are balanced results in no XPM manifests and the logical output is '0'. In contrast, when this combination, $(A + B)_{pump}$ and $(A + B)_{probe}$, is '1', which happens when either one or both of $A_{pump,\ probe}$ and $B_{pump,\ probe}$ are '1', constructive interference is created through the XGM at the output port. An OBPF is placed at the QDSOAs-TSMZI exit to reject the signals other than the switched one. A DI, which has a DI delay ($\Delta\tau$) in one of its arms and a phase bias ($\Delta\Phi$) in the other arm, is serially placed after the QDSOAs-TSMZI in order to improve the performance of the target Boolean function and make it better. The DI opens a wider phase window [45,46], which allows restoring the quality of the output gate. The output power of TSMZI passes through the DI. The DI splits this power into a clockwise component and a counterclockwise component and arrive at the 3 dB OC with the same polarization where they interfere. Therefore, the higher pattern effects are disappeared and the lower pattern effects are enhanced. In this manner, the OR operation is executed according to its truth table.

3.2. Results

In this simulation, the performance of the AO OR gate has been investigated by running Mathematica Wolfram® and using the signal and QDSOA parameters cited in Table 1 [3,6,9,15–18,256–36,45–48]. This performance has been evaluated by the QF, which

Table 1
OR simulation parameters default values [3,6,9,15–18,26–36,45–48].

Symbol	Definition	Value	Unit
E_0	Pulse energy	0.2	pJ
τ_{FWHM}	Pulse width	0.2	ps
T	Bit period	1	ps
N	PRBS length	127	–
f_A	Frequency of data A	192.4	THz
f_B	Frequency of data B	192.4	THz
f_{CW}	Frequency of CW probe	194	THz
P_A	Power of data A	2	mW
P_B	Power of data B	2	mW
P_{CW}	Power of CW probe	1	mW
P_{sat}	Saturation power	28	mW
J	Injection current density	5	kA/cm^2
τ_{wd}	Transition rate from WL to QDs state	5	ps
τ_{dw}	Excitation rate from QDs state to WL	10	ns
τ_{wr}	Carrier recombination rate in WL	2.2	ns
τ_{dr}	Carrier recombination rate in QDs state	0.4	ns
τ_{CH}	Temperature relaxation rate	0.3	ps
τ_{SHB}	Carrier-carrier scattering rate	0.1	ps
ε_{CH}	Nonlinear gain suppression factor due to CH	0.02	W^{-1}
ε_{SHB}	Nonlinear gain suppression factor due to SHB	0.02	W^{-1}
α	α-factor	4	–
α_{CH}	Linewidth enhancement factor due to CH	1	–
α_{SHB}	Linewidth enhancement factor due to SHB	0	–
Γ	Confinement factor	0.15	–
a	Differential gain	8.6×10^{-15}	cm^{-2}
d	Thickness of WL	0.5	μm
L	Length of QDSOA active region	1	mm
w	Thickness of QDSOA active region	0.3	μm
G_0	Unsaturated power gain	30	dB
f_c	Center frequency of filter	194.7	THz
B	Optical bandwidth of filter	1.8	THz
N	Order of filter	1	–
$\Delta\tau$	DI delay	0.1	ps
$\Delta\Phi$	DI phase bias	π	rad

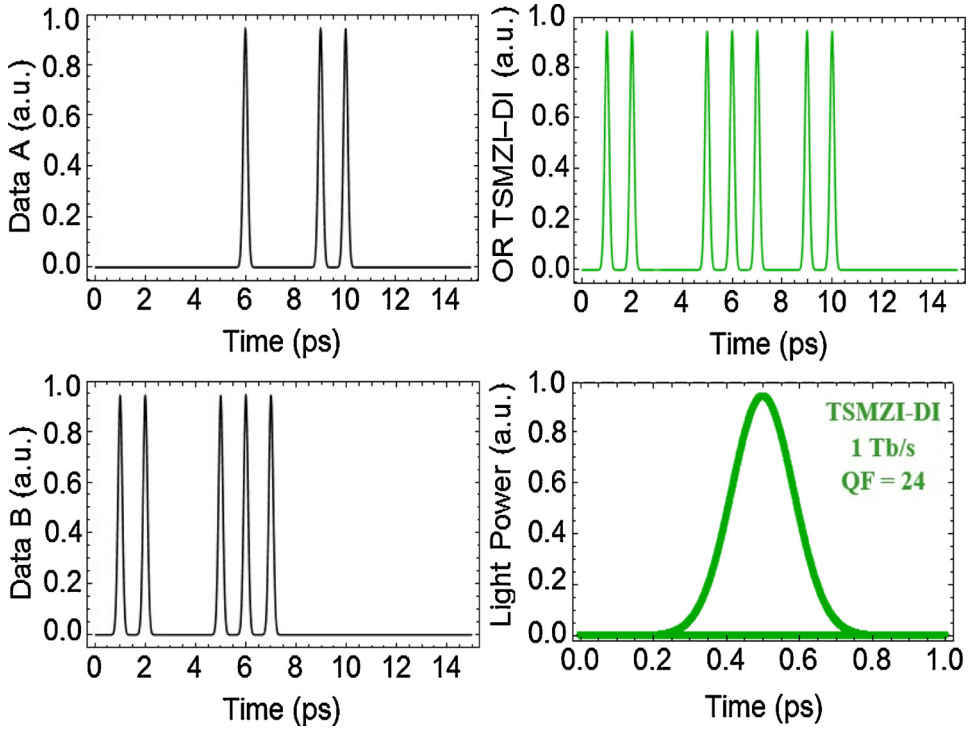

Fig. 4. OR simulation results and corresponding PED using DI after QDSOAs-TSMZI at 1 Tb/s.

is defined as $QF = (P_1 - P_0) / (\sigma_1 + \sigma_0)$ [36–38], where P_1, P_0 are the average peak powers of output signal '1' and '0' and σ_1, σ_0 are the corresponding standard deviations. This metric should be over six in order to keep the related bit-error-rate (BER) smaller than 10^{-9} [4,36]. The BER is related to the QF through $BER = (2\pi)^{-1/2} \exp[-0.5\ QF^2]/QF$ [4,5,15,37].

Figs. 4, 5 and 6 show the input data A and B as well as the OR output gate and its corresponding pseudo-eye diagrams (PED) using

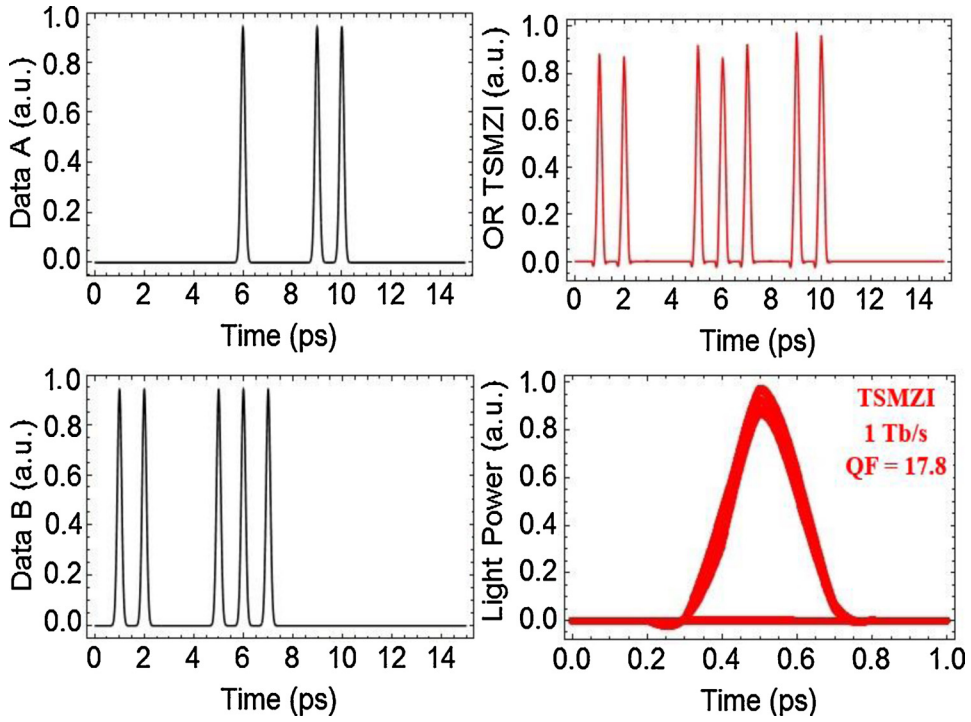

Fig. 5. OR simulation results and corresponding PED using QDSOAs-TSMZI at 1 Tb/s.

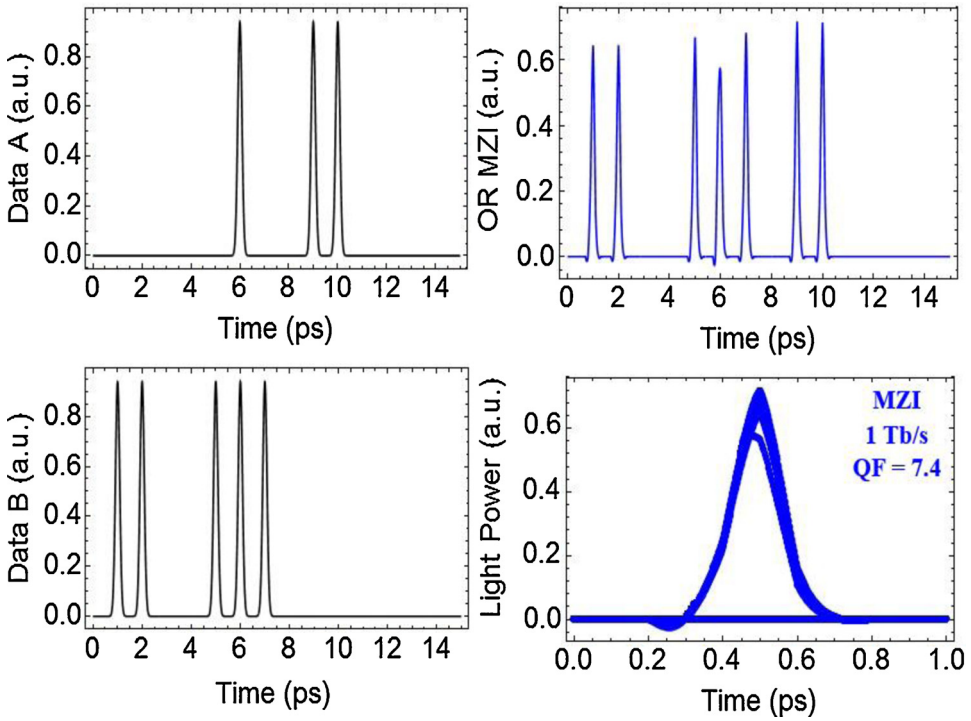

Fig. 6. OR simulation results and corresponding PED using QDSOAs-MZI at 1 Tb/s.

QDSOAs-TSMZI with a serially DI, QDSOAs-TSMZI, and QDSOAs-MZI, respectively, at 1 Tb/s. The PED using a DI after TSMZI is clearer and opener than the other schemes, which have high pattern effects. The QF using QDSOAs-TSMZI without a DI exhibits a small value, but discernible peaks with the QDSOAs-MZI. Therefore, DI improves OR performance and makes it better than using other schemes. The obtained QFs using QDSOAs-TSMZI with a serially DI, QDSOAs-TSMZI, and QDSOAs-MZI are 24, 17.8, and 7.4, respectively.

Fig. 7 confirms the active role of the DI after the TS configuration. One serially DI placed after the QDSOAs-based TSMZI can maximize the QF, which happens at $\Delta\tau$ =0.1 ps and $\Delta\Phi = \pi$. The QF is very sensitive to small changes of $\Delta\tau$, which should be carefully optimized. Furthermore, a shorter delay of 0.1 ps, which tends closer to the pulse width (0.2 ps) increases the QF.

Figs. 8 , 9 show the variation of QF against the input signal and QDSOA critical parameters include the data A, B input power (Fig. 8(a)), injection current density (Fig. 8(b), traditional linewidth enhancement factor (α-factor) (Fig. 9 (a)), and transition rate from WL to QDs GS (τ_{wd}) (Fig. 9(b)) for the OR gate at 1 Tb/s using different schemes, QDSOAs-based TSMZI followed by a DI, QDSOAs-based TSMZI, and QDSOAs-based conventional MZI. From these figures, we can observe that the exploitation of a DI after the QDSOAs-TSMZI scheme is beneficial for the OR performance for all variable parameters and the QF is much higher than QDSOAs-TSMZI and QDSOAs-MZI schemes. The input data pulses are still switched without degrading by the pattern effects induced by the

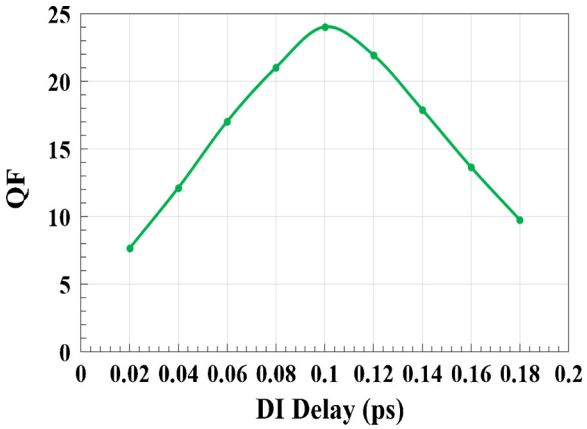

Fig. 7. OR QF vs. DI delay using QDSOAs-TSMZI-based OR gate at 1 Tb/s.

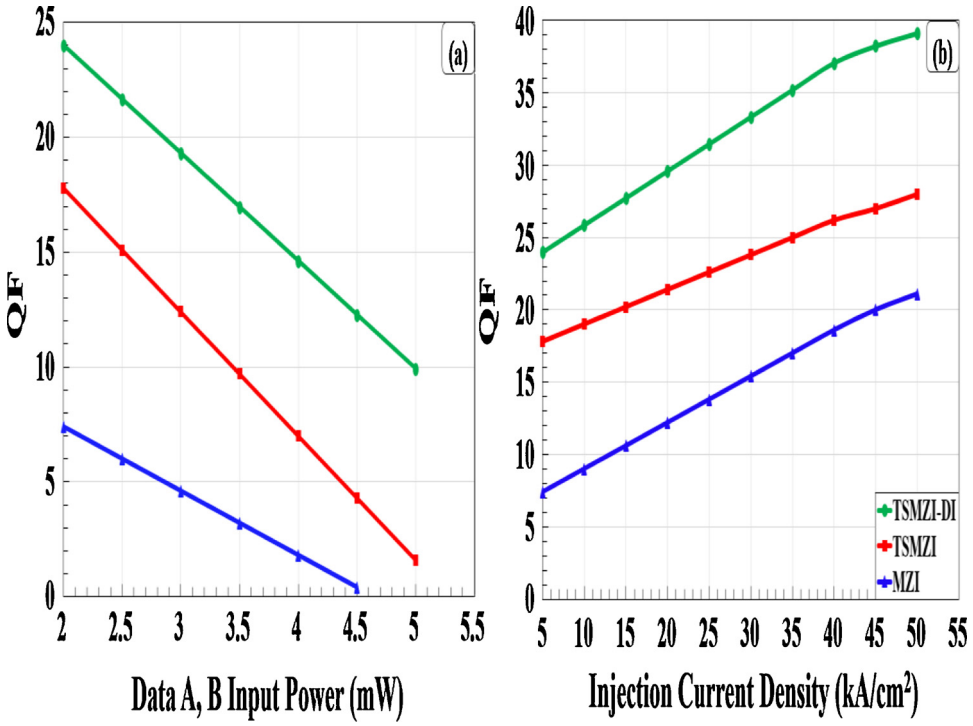

Fig. 8. OR QF vs. (a) data A, B input power and (b) injection current density using QDSOAs-TSMZI-DI, QDSOAs-TSMZI, and QDSOAs-MZI at 1 Tb/s.

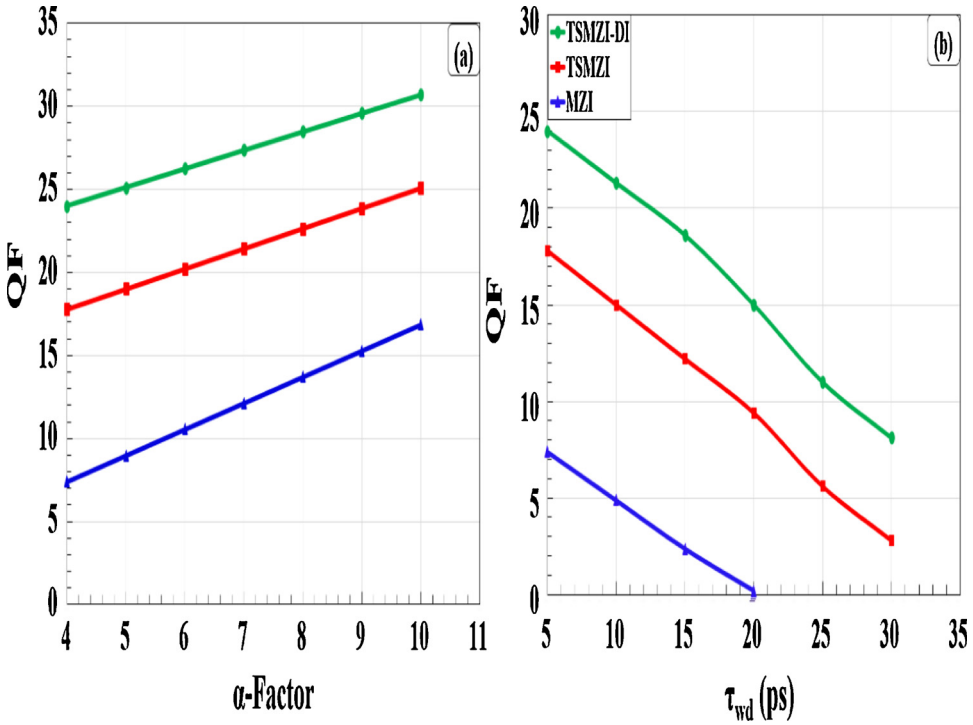

Fig. 9. OR QF vs. (a) traditional linewidth enhancement factor (α-factor) and (b) transition rate from WL to QDs GS (τ_{wd}) using QDSOAs-TSMZI-DI, QDSOAs-TSMZI, and QDSOAs-MZI at 1 Tb/s.

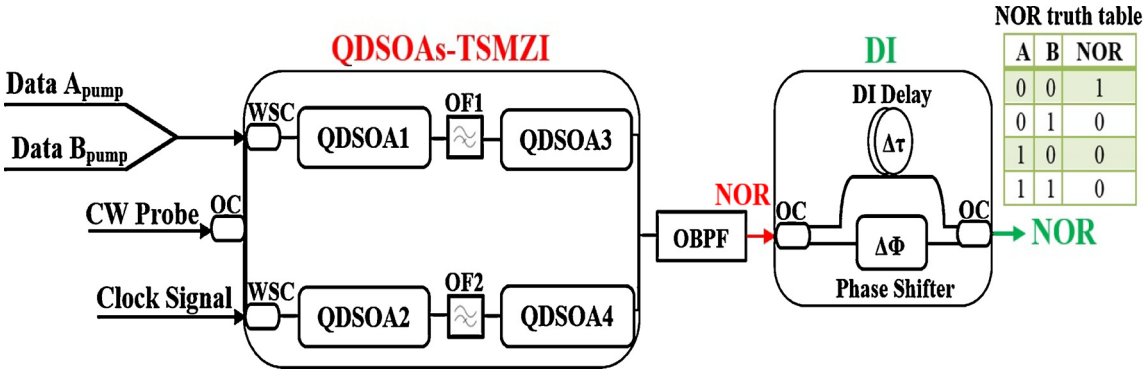

Fig. 10. Schematic diagram and truth table of NOR gate using QDSOAs-based TSMZI in series with DI.

QDSOAs heavy saturation. Practically, these characteristics are attractive as they enable to design more flexible and controllable AO operations.

4. NOR gate

4.1. Operation principle

The schematic diagram and truth table of the OA NOR gate with a DI placed in a series after QDSOAs-based TSMZI is shown in Fig. 10.

Table 2
NOR simulation parameters default values [11–18,24–36,48,49].

Symbol	Definition	Value	Unit
E_0	Pulse energy	0.2	pJ
τ_{FWHM}	Pulse width	0.2	ps
T	Bit period	1	ps
N	PRBS length	127	–
f_A	Frequency of data A	194.2	THz
f_B	Frequency of data B	194.2	THz
f_{Clk}	Frequency of clock signal	192.9	THz
f_{CW}	Frequency of CW probe	193.5	THz
P_A	Power of data A	2	mW
P_B	Power of data B	2	mW
P_{Clk}	Power of clock signal	2	mW
P_{CW}	Power of CW probe	1	mW
P_{sat}	Saturation power	9	mW
J	Injection current density	10	kA/cm^2
τ_{wd}	Transition rate from WL to QDs state	4	ps
τ_{dw}	Excitation rate from QDs state to WL	10	ns
τ_{wr}	Carrier recombination rate in WL	2.2	ns
τ_{dr}	Carrier recombination rate in QDs state	0.4	ns
τ_{CH}	Temperature relaxation rate	0.3	ps
τ_{SHB}	Carrier-carrier scattering rate	0.1	ps
ε_{CH}	Nonlinear gain suppression factor due to CH	0.02	W^{-1}
ε_{SHB}	Nonlinear gain suppression factor due to SHB	0.02	W^{-1}
α	α-factor	2	–
α_{CH}	Linewidth enhancement factor due to CH	1	–
α_{SHB}	Linewidth enhancement factor due to SHB	0	–
Γ	Confinement factor	0.15	–
a	Differential gain	8.6×10^{-15}	cm^{-2}
d	Thickness of WL	0.5	μm
L	Length of QDSOA active region	1	mm
w	Thickness of QDSOA active region	0.3	μm
G_0	Unsaturated power gain	30	dB
f_c	Center frequency of filter	194.7	THz
B	Optical bandwidth of filter	1.8	THz
N	Order of filter	1	–
Δτ	DI delay	0.1	ps
ΔΦ	DI phase bias	π	rad

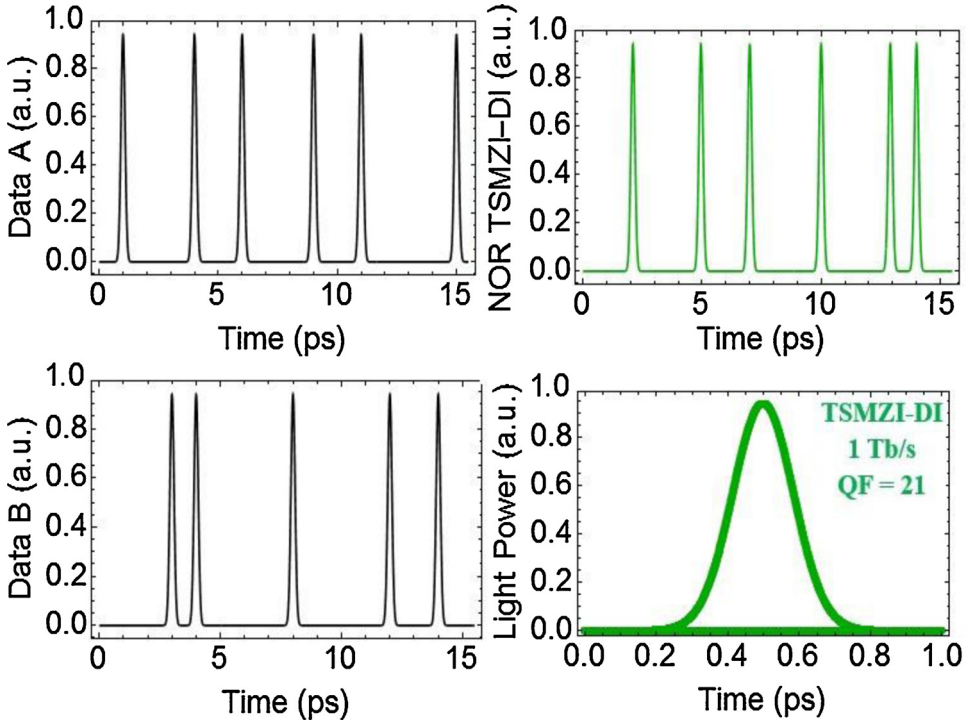

Fig. 11. NOR simulation results and corresponding PED using DI after QDSOAs-based TSMZI at 1 Tb/s.

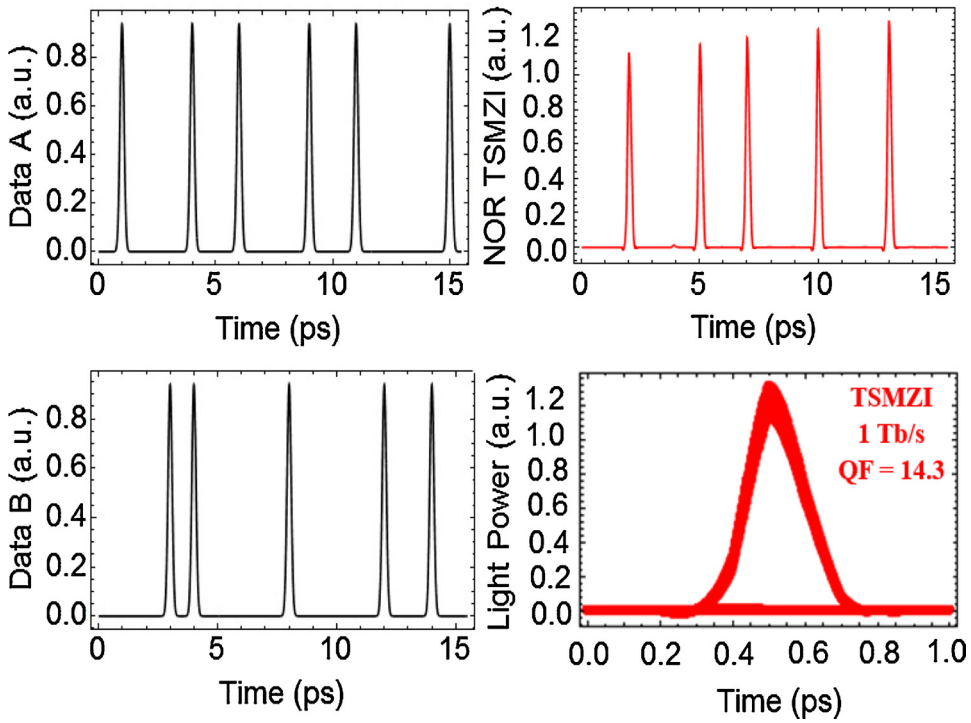

Fig. 12. NOR simulation results and corresponding PED using QDSOAs-based TSMZI at 1 Tb/s.

The input signal power inserted into QDSOA1 and QDSOA2 for the NOR operation is, respectively, described by:

$$P_{in,\ QDSOA_1}(t) = P_{A_{pump}}(t) + P_{B_{pump}}(t) + 0.5\,P_{CW} \tag{19}$$

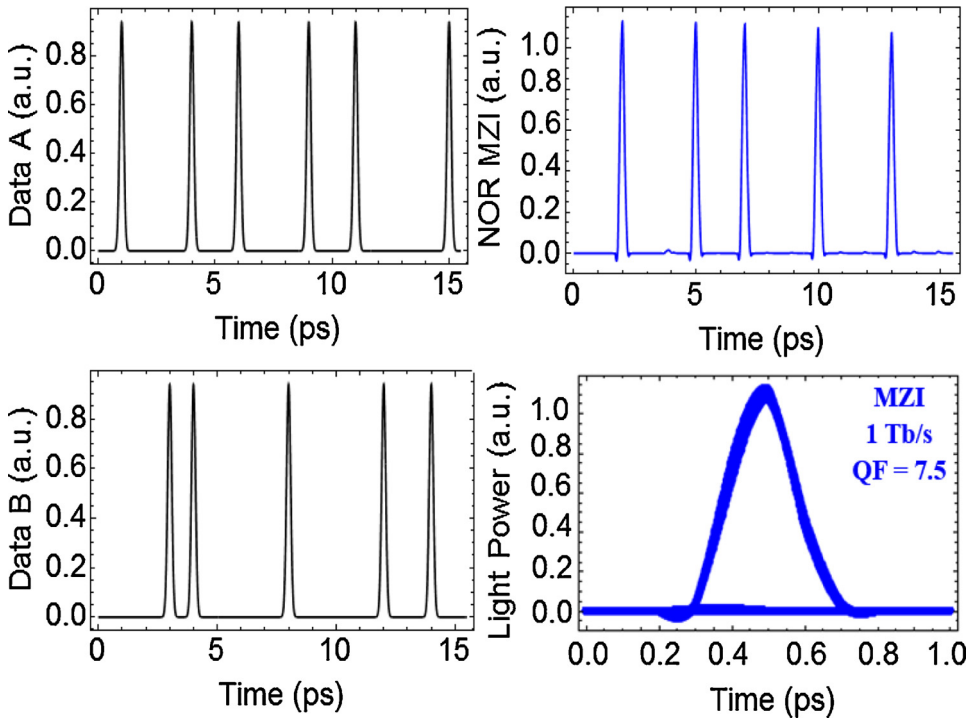

Fig. 13. NOR simulation results and corresponding PED using QDSOAs-based MZI at 1 Tb/s.

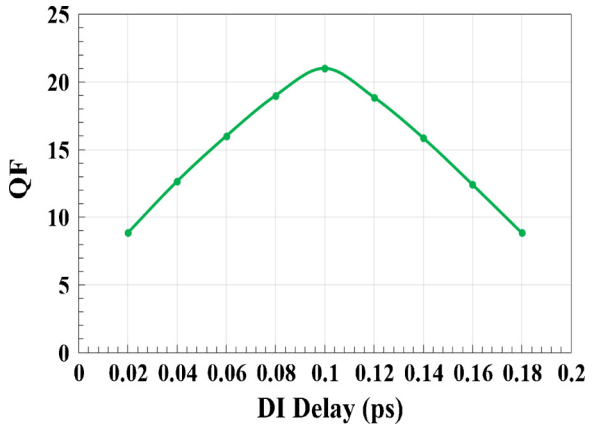

Fig. 14. NOR QF vs. DI delay using QDSOAs-TSMZI at 1 Tb/s.

$$P_{n,QDSOA_2}(t) = P_{Clk}(t) + 0.5P_{CW} \tag{20}$$

To illustrate the NOR operation, pump signals A and B as denoted by 'Data A_{pump}' and 'Data B_{pump}', respectively, are combined by the WSC and launched into the upper arm of the QDSOAs-TSMZI while a clock signal is injected in the lower arm of the QDSOAs-TSMZI. The peak powers of the pump and clock signals should be adjusted to be identical so that they give the same gain and phase modulation depth in each QDSOA [11,12]. A CW, which carries the NOR output information, is injected in the middle arm of the QDSOAs-TSMZI. When the combination of data A and B is '01', '10' or '11' inserted into the upper arm and a clock signal is all '1' launched into the lower arm, the QDSOAs get saturated and resulting in '0' at the output due to the destructive interference. On the other hand, when the combination of A and B is '00', the clock signal will break the phase balance of MZI and resulting in '1' at the output due to the constructive interference. The NOR output power of QDSOAs-TSMZI is split by the DI into a clockwise component and a counterclockwise component affected by the DI elements (i.e., $\Delta\tau$ and $\Delta\Phi$) and arrive at the 3 dB OC with the same polarization where they interfere. In this manner, the NOR gate is executed with better performance, according to its truth table.

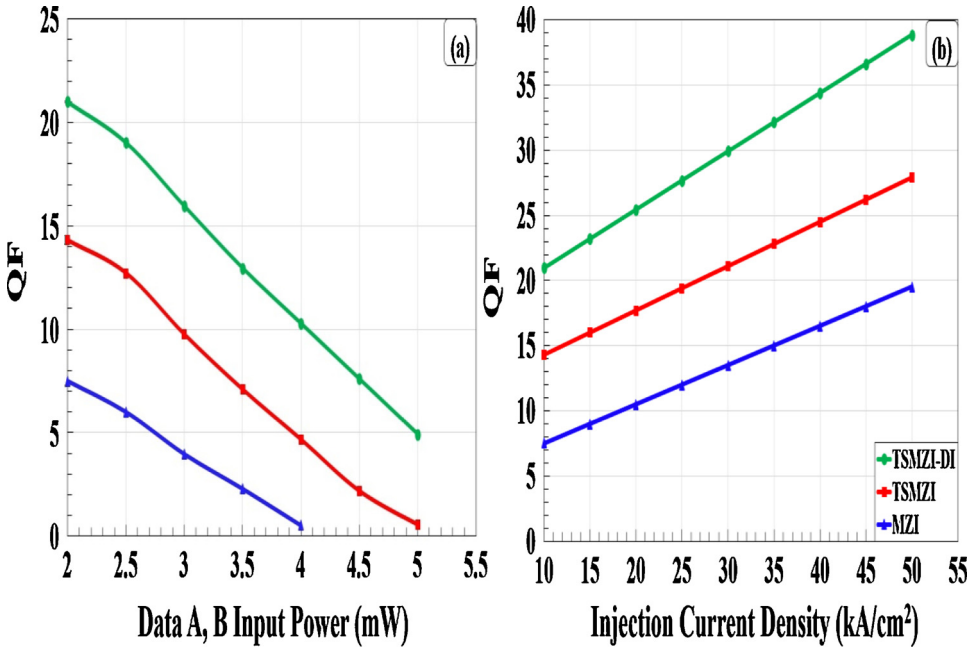

Fig. 15. NOR QF vs. (a) data A, B input power and (b) injection current density using QDSOAs-TSMZI-DI, QDSOAs-TSMZI, and QDSOAs-MZI at 1 Tb/s.

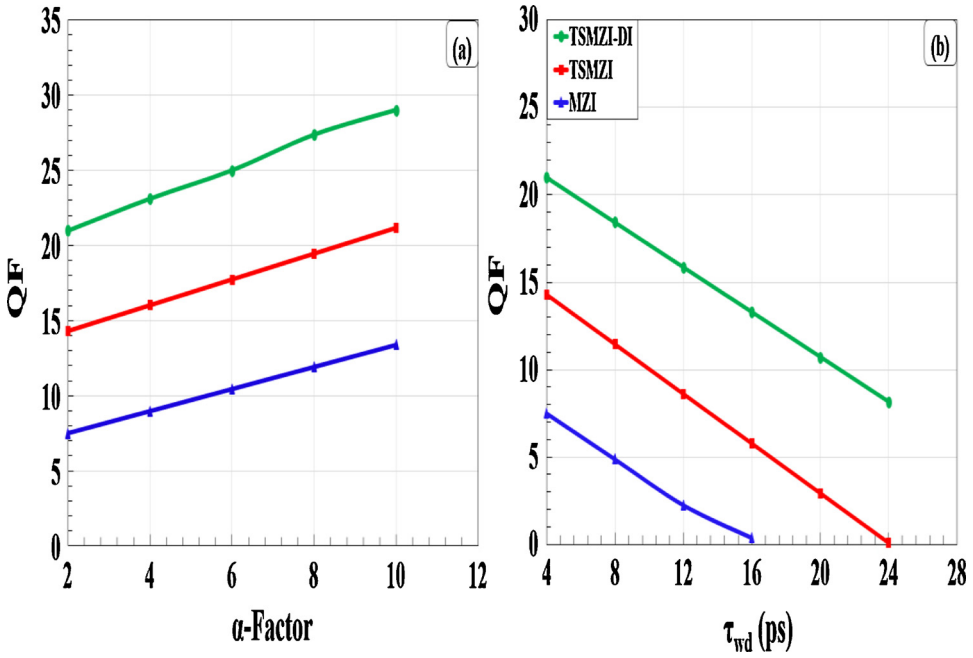

Fig. 16. NOR QF vs. (a) traditional linewidth enhancement factor (α-factor) and (b) transition rate from WL to QDs GS (τ_{wd}) using QDSOAs-TSMZI-DI, QDSOAs-TSMZI, and QDSOAs-MZI at 1 Tb/s.

4.2. Results

The input signal and QDSOA parameters used for the NOR gate are cited in Table 2 [11–18,24–36,48,49]. The performance of the NOR gate is also evaluated by the QF.

Figs. 11, 12, 13 show the simulation results and corresponding PED for the NOR gate using a DI after the QDSOAs-based TSMZI, QDSOAs-based TSMZI, and QDSOAs-based conventional MZI, respectively, at 1 Tb/s. The input A, B, and clock patterns are Gaussian-shaped with 127 pseudorandom data pattern. The obtained QF using a serially DI after the QDSOAs-TSMZI is 21 compared with 14.3

and 7.5 when using QDSOAs-TSMZI and QDSOAs-MZI, respectively.

Fig. 14 shows the QF dependence on the DI delay for the NOR function using QDSOAs-TSMZI followed by a series DI at 1 Tb/s. The value of the QF coming out of the DI depends on the DI elements, i.e., $\Delta\tau$ and $\Delta\Phi$. The QF has a maximum value of 21 at $\Delta\tau = 0.1$ ps and $\Delta\Phi = \pi$.

Figs. 15 and 16 illustrate the QF against the input signal and QDSOA critical parameters include the data A, B input power as shown in Fig. 15(a), injection current density as shown in Fig. 15(b), α-factor as shown in Fig. 16 (a), and τ_{wd} as shown in Fig. 16(b) for the OR gate at 1 Tb/s using different schemes, QDSOAs-based TSMZI followed by a DI, QDSOAs-based TSMZI, and QDSOAs-based conventional MZI. It can be seen that the QF remains high across the whole scanned span using QDSOAs-TSMZI followed by a DI, while this extent is lower when using QDSOAs-TSMZI and QDSOAs-MZI.

5. Conclusion

We studied the performance of all-optical OR and NOR logic operations using quantum-dot semiconductor optical amplifiers (QDSOAs)-assisted turbo-switched Mach-Zehnder interferometer (TSMZI) followed by a serially delayed interferometer (DI) at 1 Tb/s data rate. The variation of the quality factor (QF) against the input signal and QDSOA critical parameters was investigated and assessed. The obtained results indicate that connecting a DI in series with QDSOAs-assisted TSMZI renders a higher QF at 1 Tb/s rather than in both TSMZI and MZI schemes.

Declaration of interests

The authors declare that they have no known competing financial interests or personal relationships that could have appeared to influence the work reported in this paper.

Acknowledgments

This work was funded by the Chinese Academy of Sciences President's International Fellowship Initiative (PIFI) (Grant No. 2019FYT0002) and Talented Young Scientist Program (TYSP) supported by the China Science and Technology Exchange Center of Ministry of Science and Technology of China.

References

[1] J. Mørk, M.L. Nielsen, T.W. Berg, The dynamics of semiconductor optical amplifiers: modeling and applications, Opt. Photon. News 14 (2003) 42–48.
[2] A. Kotb, C. Guo, Two-photon absorption in quantum-dot semiconductor optical amplifiersbased all-optical XOR gate at 2 Tb/s, Opt. Quantum Electron. 51 (2019) 1–12.
[3] A. Kotb, K.E. Zoiros, C. Guo, 2 Tb/s all-optical gates based on two-photon absorption in quantum-dot semiconductor optical amplifiers, Opt. Laser Technol. 112 (2019) 442–451.
[4] S. Thapa, X. Zhang, N.K. Dutta, Effects of two-photon absorption on pseudo-random bit sequence operating at high speed, J. Mod. Opt. 66 (2019) 100–108.
[5] X. Zhang, N.K. Dutta, Effects of two-photon absorption on all-optical logic operation based on quantum-dot semiconductor optical amplifiers, J. Mod. Opt. 166 (2018) 166–175.
[6] A. Kotb, Simulation of high-quality-factor all-optical logic gates based on quantum-dot semiconductor optical amplifier at 1 Tb/s, Optik 126 (2016) 320–325.
[7] A. Kotb, Modeling of high-quality-factor XNOR gate using quantum-dot semiconductor optical amplifiers at 1 Tb/s, Rev. Bras. Fisioter. 45 (2015) 288–295.
[8] A. Kotb, K.E. Zoiros, 1 Tb/s high-quality factor NAND gate using quantum-dot semiconductor optical amplifiers in Mach–Zehnder interferometer, J. Comp. Electron. 13 (2014) 555–561.
[9] A. Kotb, K.E. Zoiros, On the design of all-optical gates based on quantum-dot semiconductor optical amplifier with effect of amplified spontaneous emission, Opt. Quantum Electron. 46 (2014) 977–989.
[10] A. Kotb, K.E. Zoiros, Simulation of all-optical logic XNOR gate based on quantum-dot semiconductor optical amplifiers with amplified spontaneous emission, Opt. Quantum Electron. 45 (2013) 1213–1222.
[11] A. Kotb, NOR gate based on QD-SOA at 250 Gbit/s, Opt. Quantum Electron. 45 (2013) 473–480.
[12] A. Kotb, 1 Tb/s high-quality factor NOR gate based on quantum-dot semiconductor optical amplifier, Opt. Quantum Electron. 45 (2013) 1258–1268.
[13] E. Dimitriadou, K.E. Zoiros, On the design of reconfigurable ultrafast all-optical NOR and NAND gates using a single quantum-dot semiconductor optical amplifier-based Mach-Zehnder interferometer, J. Opt. 14 (2012) 105401.
[14] E. Dimitriadou, K.E. Zoiros, Proposal for all-optical NOR gate using single quantum-dot semiconductor optical amplifier-based Mach-Zehnder interferometer, Opt. Commun. 285 (2012) 1710–1716.
[15] S. Ma, Z. Chen, H. Sun, N.K. Dutta, High-speed all-optical logic gates based on quantum-dot semiconductor optical amplifiers, Opt. Express 18 (2010) 6417–6422.
[16] A. Rostami, H. Nejad, R. Qartavol, H. Saghai, Tb/s optical logic gates based on quantum-dot semiconductor optical amplifiers, IEEE J. Quantum Electron. 46 (2010) 354–360.
[17] Y. Ben-Ezra, B.I. Lembrikov, M. Haridim, Ultrafast all-optical processor based on quantum-dot semiconductor optical amplifiers, IEEE J. Quantum Electron. 45 (2009) 34–41.
[18] H. Sun, Q. Wang, H. Dong, N.K. Dutta, All-optical logic performance of quantum-dot semiconductor amplifier based devices, Microwave Opt. Technol. Lett. 48 (2006) 29–35.
[19] N. Yasuoka, K. Kawaguchi, H. Ebe, T. Akiyama, M. Ekawa, K. Morito, M. Sugawara, Y. Arakawa, Quantum-dot semiconductor optical amplifiers with polarization-independent gains in 1.5-μm wavelength bands, IEEE Photonics Technol. Lett. 20 (2008) 1908–1910.
[20] T. Akiyama, M. Ekawa, M. Sugawara, K. Kawaguchi, H. Sudo, A. Kuramata, H. Ebe, Y. Arakawa, An ultrawide-band semiconductor optical amplifier having an extremely high penalty-free output power of 23 dBm achieved with quantum-dots, IEEE Photon, Technol. Lett. 17 (2005) 1614–1616.
[21] T.W. Berg, J. Mørk, Saturation and noise properties of quantum-dot optical amplifiers, IEEE J. Quantum Electron. 40 (2004) 1527–1539.
[22] A.H. Flayyih, A.H. Al-Khursan, Theory of pulse propagation and four-wave mixing in a quantum-dot semiconductor optical amplifier, Curr. Appl. Phys. 14 (2014) 946–953.
[23] A.J. Zilkie, J. Meier, M. Mojahedi, P.J. Poole, P. Barrios, D. Poitras, T.J. Rotter, C. Yang, A. Stintz, K.J. Malloy, P.W.E. Smith, J.S. Aitchison, Carrier dynamics of quantum-dot, quantum-dash, and quantum-well semiconductor optical amplifiers operating at 1.55 μm, IEEE J. Quantum Electron. 43 (2007) 982–991.

[24] R.J. Manning, X. Yang, R.P. Webb, R. Giller, F.C.G. Gunning, A.D. Ellis, The “turbo-switch” – a novel technique to increase the high-speed response of SOAs for wavelength conversion, Proc. Optical Fiber Communications Conference (2006).
[25] R.J. Manning, R. Giller, X. Yang, R.P. Webb, D. Cotter, Faster switching with semiconductor optical amplifiers, Proc. Photonics in Switching (2007).
[26] I. Rendón-Salgado, E. Ramírez-Cruz, R. Gutiérrez-Castrejón, 640 Gb/s all-optical AND gate and wavelength converter using bulk SOA turbo–switched Mach–Zehnder interferometer with improved differential scheme, Opt. Laser Technol. 109 (2019) 671–681.
[27] I. Rendón-Salgado, R. Gutiérrez-Castrejón, 160 Gb/s all-optical AND gate using bulk SOA turbo–switched Mach–Zehnder interferometer, Opt. Commun. 399 (2017) 77–86.
[28] X. Yang, W. Hu, Principle and applications of semiconductor optical amplifiers-based turbo-switches, Front. Optoelectron. China 9 (2016) 346–352.
[29] Q. Weng, X. Yang, W. Hu, Theoretical analysis of high-speed all-optical turbo-switches, IEEE J. Sel. Top. Quantum Electron. 18 (2012) 662–669.
[30] R. Gutiérrez-Castrejón, Turbo-switched Mach-Zehnder interferometer as all-optical signal processing element at 160 Gb/s, Opt. Commun. 282 (2009) 4345–4352.
[31] A. Kotb, C. Guo, Theoretical implementation of all-optical XOR gate at 160 Gb/s using semiconductor optical amplifiers-based turbo-switched Mach-Zehnder interferometer, Adv. Opt. Photon. 1 (2018) 263–278.
[32] H. Sun, Q. Wang, H. Dong, Z. Chen, N.K. Dutta, J. Jaques, A.B. Piccirilli, All-optical logic XOR gate at 80 Gb/s using SOA-MZI-DI, IEEE J. Quantum Electron. 42 (2006) 747–751.
[33] S. Randel, A.M. Melo, K. Petermann, V. Marembert, C. Schubert, Novel scheme for ultrafast all-optical XOR operation, J. Lightwave Technol. 22 (2004) 2808–2815.
[34] A. Kotb, K.E. Zoiros, C. Guo, 320 Gb/s all-optical XOR gate using semiconductor optical amplifier-Mach-Zehnder interferometer and delayed interferometer, Photon. Netw. Commun. 38 (2019) 177–184.
[35] R. Gutiérrez-Castrejón, M. Dülk, S. Fischer, G. Guekos, Novel scheme for optical time-division demultiplexing using a delayed interferometer, Opt. Commun. 192 (2001) 245–254.
[36] A. Kotb, K.E. Zoiros, C. Guo, 1 Tb/s all-optical XOR and AND gates using quantum-dot semiconductor optical amplifier-based turbo-switched Mach-Zehnder interferometer, J. Comp. Electron. 18 (2019) 628–639.
[37] N.K. Dutta, Q. Wang, Semiconductor Optical Amplifiers, 2nd ed., World Scientific Publishing Company, Singapore, 2013.
[38] A. Kotb, All-Optical Logic Gates Using Semiconductor Optical Amplifier, Lambert Academic Publishing, Saarbrucken, 2012.
[39] D. Breuer, K. Petermann, Comparison of NRZ- and RZ-modulation format for 40-Gb/s TDM standard-fiber systems, IEEE Photonics Technol. Lett. 9 (1997) 398–400.
[40] K. Komatsu, G. Hosoya, H. Yashima, All-optical logic NOR gate using a single quantum-dot SOA-assisted an optical filter, Opt. Quantum Electron. 50 (2018) 131.
[41] G.P. Agrawal, N.A. Olsson, Self-phase modulation and spectral broadening of optical pulses in semiconductor laser amplifiers, IEEE J. Quantum Electron. 25 (1989) 2297–2306.
[42] D. Cassioli, S. Scotti, A. Mecozzi, A time-domain computer simulator of the nonlinear response of semiconductor optical amplifiers, IEEE J. Quantum Electron. 36 (2000) 1072–1080.
[43] A. Yariv, Universal relations for coupling of optical power between microresonators and dielectric waveguides, Electron. Lett. 36 (2000) 321–322.
[44] K.E. Zoiros, C. Demertzis, On the data rate extension of semiconductor optical amplifier-based ultrafast nonlinear interferometer in dual rail switching mode using a cascaded optical delay interferometer, Opt. Laser Technol. 43 (2011) 1190–1197.
[45] Q. Wang, H. Dong, H. Sun, N.K. Dutta, All-optical logic OR gate using SOA delayed interferometer, Opt. Commun. 260 (2006) 81–86.
[46] H. Dong, Q. Wang, G. Zhu, J. Jaques, A.B. Piccirilli, N.K. Dutta, Demonstration of all-optical OR gate using semiconductor optical amplifier-delayed interferometer, Opt. Commun. 242 (2004) 479–485.
[47] A. Kotb, K.E. Zoiros, C. Guo, Numerical investigation of all-optical logic OR gate at 80 Gb/s with dual pump-probe semiconductor optical amplifier (SOA)-assisted Mach-Zehnder interferometer (MZI), J. Comp. Electron. 18 (2019) 271–278.
[48] J. Dong, X. Zhang, J. Xu, D. Huang, 40 Gb/s all-optical logic NOR and OR gates using a semiconductor optical amplifier: experimental demonstration and theoretical analysis, Opt. Commun. 281 (2008) 1710–1715.
[49] J. Xu, X. Zhang, D. Liu, D. Huang, Ultrafast all-optical NOR gate based on semiconductor optical amplifier and fiber delay interferometer, Opt. Express 14 (2006) 10708–10714.